RESEARCH ARTICLE | APRIL 23 2025

Designs for scalable construction of hybrid quantum photonic cavities

Andrew S. Greenspon ; Mark Dong ; Ian Christen; Gerald Gilbert; Matt Eichenfield ; Dirk Englund

APL Quantum 2, 026110 (2025)
https://doi.org/10.1063/5.0242498

Designs for scalable construction of hybrid quantum photonic cavities

Cite as: APL Quantum 2, 026110 (2025); doi: 10.1063/5.0242498
Submitted: 30 January 2025 • Accepted: 6 March 2025 •
Published Online: 23 April 2025

Andrew S. Greenspon,[1,2,a] Mark Dong,[1,2,b] Ian Christen,[2] Gerald Gilbert,[3] Matt Eichenfield,[4,5] and Dirk Englund[2,6,c]

AFFILIATIONS

[1] The MITRE Corporation, 202 Burlington Road, Bedford, Massachusetts 01730, USA
[2] Research Laboratory of Electronics, Massachusetts Institute of Technology, Cambridge, Massachusetts 02139, USA
[3] The MITRE Corporation, 200 Forrestal Road, Princeton, New Jersey 08540, USA
[4] Sandia National Laboratories, P.O. Box 5800, Albuquerque, New Mexico 87185, USA
[5] College of Optical Sciences, University of Arizona, Tucson, Arizona 85719, USA
[6] Brookhaven National Laboratory, 98 Rochester St, Upton, New York 11973, USA

[a] Author to whom correspondence should be addressed: agreenspon@mitre.org
[b] mdong@mitre.org
[c] englund@mit.edu

ABSTRACT

Nanophotonic resonators are central to numerous applications, from efficient spin–photon interfaces to laser oscillators and precision sensing. A leading approach consists of photonic crystal (PhC) cavities, which have been realized in a wide range of dielectric materials. However, translating proof-of-concept devices into a functional system entails a number of additional challenges, inspiring new approaches that combine resonators with wavelength-scale confinement and high quality factors; scalable integration with integrated circuits and photonic circuits; electrical or mechanical cavity tuning; and, in many cases, a need for heterogeneous integration with functional materials such as III–V semiconductors or diamond color centers for spin–photon interfaces. Here we introduce a concept that generates a finely tunable PhC cavity at a selected wavelength between two heterogeneous optical materials whose properties satisfy the above requirements. The cavity is formed by stamping a hard-to-process material with simple waveguide geometries on top of an easy-to-process material consisting of dielectric grating mirrors and active tuning capability. We simulate our concept for the particularly challenging design problem of multiplexed quantum repeaters based on arrays of cavity-coupled diamond color centers, achieving theoretically calculated unloaded quality factors of 10^6, mode volumes as small as $1.2(\lambda/n_{eff})^3$, and maintaining >60% total on-chip collection efficiency of fluorescent photons. We further introduce a method of low-power piezoelectric tuning of these hybrid diamond cavities, simulating optical resonance shifts up to ~760 GHz and color center fluorescence tuning of 5 GHz independent of cavity tuning. These results will motivate integrated photonic cavities toward larger scale systems-compatible designs.

INTRODUCTION

Photonic crystal (PhC) cavities are ubiquitous in optics, with applications including modulation,[1] spectroscopy,[2] filtering,[3,4] sensing,[5,6] lasers, nonlinear optics,[7] and coupling to quantum emitters.[8] Particularly in quantum information processing, PhC cavities are useful for improving optical coupling to atomic systems that include color centers in diamond[9–12] and silicon carbide,[13] quantum dots in III–V semiconductors,[14,15] or other atoms in other solid state systems.[16,17] Moreover, widely tunable cavity resonances with stable embedded quantum emitters simplify the practical generation of identical photons for remote-entanglement operations necessary for creating quantum networks or network-based quantum computers.[18] Monolithic diamond PhC cavities have been fabricated

with high quality factor,[19] demonstrating Purcell enhancement[20] of the emission from implanted nitrogen vacancies (NVs)[21] and group–IV color centers.[9,10,22] Other reported plasmonic–photonic cavities[23] for near-surface NVs have a simulated mode volume of $\sim 0.1(\lambda/n)^3$. Additional hybrid cavities have been constructed by patterning high index cavities, usually microdisks, that are then transferred to bulk diamond.[24–26] Hybrid cavities have also been constructed with other materials such as silicon and III–V semiconductors.[27–29]

However, scalable and repeatable fabrication of nanoscale features to define cavities remains difficult, especially in materials that either lack mature processing techniques, are limited to small substrates, or when short optical wavelengths are required. In diamond cavities, color centers are often placed too close to nearby patterned surfaces, which can have lattice damage from plasma etching[30] or create unwanted surface state dynamics.[31,32] Variations in surface states and other defect states may cause ionization of the color centers from the spin-active negatively charged state to a neutral state,[33] along with spectral broadening and diffusion,[34] and a decrease in spin coherence time.[35,36] Moreover, cavities composed of non-CMOS-compatible dielectrics can be difficult to integrate into large-scale, CMOS-fabricated photonic integrated circuits (PICs) and may require optical isolation from the substrate to avoid low quality factor and high losses into the substrate. The optimal placement of the emitter at the high-field location to optimize Purcell enhancement is a stochastic process.[12]

In this work, we propose a hybrid PhC cavity concept that addresses several challenges of scalable cavity fabrication. The design consists of two parts: (1) a functional dielectric or semiconductor (III–V or quantum material) patterned into a simple waveguide and (2) a CMOS-fabricated target substrate with high-resolution grating mirrors and cavity tuning capabilities made with standardized processing techniques. By heterogeneously stamping material 1 onto material 2, we not only improve the overall fabrication precision but also enable a tailorable cavity with an optical mode based on pre-selected devices. We particularly consider the application to cavity-enhanced spin–photon interfaces in quantum information processing applications. We show through simulations that by simply placing color centers in diamond waveguide "quantum microchiplets" (QMCs) onto a patterned silicon nitride (SiN) nanostructure, we can form hybrid PhC cavities with high quality factors ($Q > 10^6$) and small mode volumes [$V \sim 1.2\ (\lambda/n_{eff})^3$]. Diamond waveguides place color centers further from potential etch damage and surface state effects as compared to monolithic diamond cavities. Color centers within these as-fabricated chiplets and via similar waveguide fabrication methods have shown near-lifetime limited linewidths in several studies.[9,37]

We also calculate cavity out-coupling via the diamond waveguide with a theoretical Purcell enhancement of >895 with 90.5% of the light emitted into the desired optical mode for photon routing via an underlying PIC. Finally, we simulate the integration of these cavities with a piezoelectrically actuated photonics platform,[38] enabling

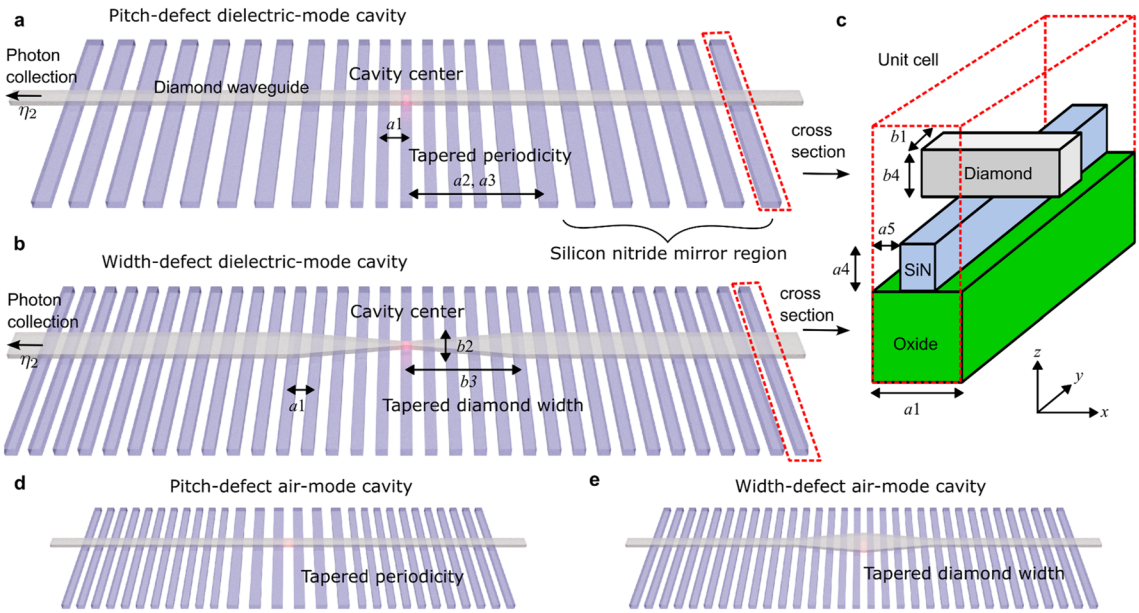

FIG. 1. General design of a hybrid cavity. A hybrid cavity is composed of a diamond waveguide placed on top of a dielectric (silicon nitride) grating. These two structures combined form a hybrid photonic crystal cavity. (a) Schematic of a pitch-defect cavity geometry for a dielectric optical mode where the SiN mirrors have a tapered periodicity starting from narrow at the cavity center to wider at the edges. (b) Schematic of a width-defect cavity geometry for a dielectric optical mode where the diamond waveguide width is tapered starting from narrow at the cavity center to wider at the edges. (c) Unit cell of a hybrid cavity with a diamond nanobeam, patterned SiN structures, and an underlying SiO_2 on a Si substrate. The cavity modes can be tuned by multiple geometric parameters, including diamond height *b*4, width *b*1, width tapering *b*2, *b*3, central grating pitch *a*1, grating taper length *a*2, *a*3, SiN height *a*4, and grating fill factor *a*5. (d) and (e) Schematics of the corresponding air optical modes of pitch-defect and width-defect hybrid cavities, respectively. In these cases, the pitch-defect and waveguide widths are tapered starting from larger at the cavity center to smaller at the edges.

low-power piezoelectric tuning of both the cavity mode (>760 GHz) and color center emission spectrum (5 GHz independent of cavity tuning, up to 50 GHz with cavity-dependent tuning) through strain and moving boundary effects. This tuning capability should improve the yield of identical spin-active emitters for high-fidelity quantum information processing.

HYBRID CAVITY CONCEPTS AND DESIGNS

The general design of the PhC hybrid cavity is shown in Fig. 1. A pre-etched nanostructure containing quantum emitters, such as any dielectric or semiconductor material waveguide, is heterogeneously integrated via direct placement on a patterned layer stack on a silicon wafer. For our particular geometry, we assume a diamond waveguide placed (along the x direction) on a substrate consisting of SiN on top of a thick layer of SiO_2.

Experimentally, arrays of diamond waveguides can be fabricated via a previously well-described process.[37,39] Such "quantum microchiplets" are attached to a diamond substrate via tethers. Tungsten probes can be used to break these tethers to transfer the QMC to a PDMS stamp with the smoother top surface facing up. The QMC on the PDMS stamp is then flipped over, and an optical microscope can be used to align the chiplet to the SiN nanolines, as demonstrated in previous work.[40]

Confinement of the optical mode is naturally achieved by the diamond waveguide in the lateral (y) and vertical (z) directions while the evanescent field interacts with the underlying SiN. The SiN is patterned to form lines alternating with air with a specified pitch and fill factor to create a bandgap between allowed frequency bands in the hybridized diamond–SiN system—here the bands are the canonical air and dielectric modes of a periodic structure. Within the gap, no optical band is supported, so the system acts as a mirror. In this hybrid architecture, a cavity is formed by varying device parameters such that a band—either air or dielectric—becomes locally allowed. Outside of this varied region, the system returns to the mirror state, leaving an island of confinement amid the mirror.

In our designs, we use a parabolic[41] variation of either the diamond waveguide width (width defect) or grating pitch (pitch defect) to locally tune the band and create the cavity. There are thus four distinct cavity configurations depending on whether the width or pitch is used to create the defect and toward which allowed band the defect is tuned, each of which may be preferred depending on the physical situation: (i) pitch defect dielectric mode where the pitch increases from the center, confining the optical mode in the diamond and underlying SiN regions; (ii) pitch defect air mode where the pitch decreases from the center, confining the optical mode in the diamond and underlying air regions; (iii) width defect dielectric mode where the diamond width increases from the center, confining the optical mode in the diamond and underlying SiN regions; (iv) width defect air mode where the diamond width decreases from the center, confining the optical mode in the diamond and underlying air regions. We note that, in all designs, the underlying patterned lines have an important translation invariant symmetry in the longitudinal (y) direction, allowing greater tolerance in aligning the diamond waveguide during heterogeneous integration.

There are several geometric parameters that can be varied in this system for achieving the desired cavity mode. We define each of the geometric parameters in a set $\{a1, a2, a3, a4, a5, b1, b2, b3, b4\}$ with definitions given in Table I. For a pitch defect cavity, $a2$ and $a3$ are varied while $b2$ and $b3$ are set to 0 (vice versa for a width defect). The pitch defect varies according to $a^{(j)} = a1 + a2(j/a3)^2$, where $a^{(j)}$ is the pitch at the jth position away from a central pitch $a1$, $a3$ is the number of periods over which the pitch changes by $a2$. After $a3$ periods, the remaining lines have pitch $a1 + a2$ for the mirror section. For a width defect, the equation is similar except the variation in waveguide width is given by a continuous coordinate (instead of discrete), which defines the parabolic curve variation between the central and mirror width sections.

For general quantum networking applications, two important cavity parameters must be optimized: the spectral efficiency η_1 and the collection efficiency η_2, which combine to make up the total efficiency $\eta_{tot} = \eta_1\eta_2$. These efficiencies are critical for the scalable processing of the emitted single photons or executing

TABLE I. List of geometric parameters for SiN lines and diamond waveguide to generate hybrid cavities.

Variable	Definition
	SiN line parameters (pitch-defect)
$a1$	Central grating pitch
$a2$	Change in pitch from center to mirror over taper region
$a3$	Number of periods in taper
$a4$	SiN thickness
$a5$	Grating fill factor
	Diamond waveguide parameters (width-defect)
$b1$	Waveguide center width
$b2$	Change in waveguide width from center to mirror over taper region
$b3$	Length of waveguide taper
$b4$	Waveguide height

remote-entanglement protocols. Specifically, we consider the case of spin-selective photon emission from color centers in diamond. The process is generally inefficient ($\eta_1 \ll 1$) due to significant emission into the phonon sideband (PSB) (e.g., 0.96 for NVs[42] and 0.4 for SnV[43]) instead of the zero-phonon line (ZPL). Moreover, once the fluorescent photon is emitted into the cavity, efficient outcoupling (η_2) through a PIC or free-space for processing becomes critical. The cavity must be maximized for both parameters. The spectral efficiency η_1 is defined as[44]

$$\eta_1 = F/\left(F + \frac{\Gamma_{total,0}}{\Gamma_{ZPL,0}} - 1\right), \tag{1}$$

where $F = \frac{3}{4\pi}(\lambda/n_{eff})^3(Q/V)$ is the Purcell factor of the ZPL emission at a wavelength λ within a cavity of quality factor Q, mode volume V, and effective refractive index n_{eff}, $\Gamma_{total,0}$ is the emitter's total emission rate without cavity enhancement, and $\Gamma_{ZPL,0}$ is the emission rate into the ZPL absent cavity enhancement. The straightforward strategy is simply to maximize the cavity Q while reducing the mode volume V to improve spectral efficiency. However, adjusting the cavity geometry to increase collection efficiency η_2 generally decreases quality factor Q, as the emitter photons cycle less in the cavity before exiting the desired collection path. For a cavity with a very large number of mirror sections on both sides, Q will be high (with equivalent high F and η_1 approaching 1), but outcoupling will suffer. The key design challenge is to proportionally decrease the mirror reflectivity (and hence the cavity Q) to increase outcoupling η_2 while maintaining a high spectral efficiency η_1 to maximize the figure of merit (FoM) η_{tot}.[45] To estimate an acceptable value of the Purcell factor that will enable a high η_1, we insert the Debye–Waller factors (0.04, 0.7, and 0.6 for the NV-, SiV-, and SnV-, respectively) into Eq. (1). These inputs lead to total $\frac{\Gamma_{total,0}}{\Gamma_{ZPL,0}} - 1$ values of 24, 0.43, and 0.67, respectively. Therefore, a relatively small Purcell factor of even 10 can bring η_1 to 96% and 94% for the SiV- and SnV- (for NV-, a Purcell >100 is required). By assuming a typical normalized mode volume for PhC cavities on the order of $V \sim 1.0(\lambda/n_{eff})^3$, we find that cavity Qs need only reach ~100–1000 to maintain a high spectral efficiency. Finally, by adjusting the cavity mirrors appropriately, we then optimize the outcoupling efficiency η_2.

HYBRID CAVITY OPTICAL SIMULATION RESULTS

We proceed to design and simulate optimal cavity designs for diamond color centers using several 3D numerical simulation tools. We generally follow the design philosophy of erring on the side of nanofabrication simplicity. Therefore, because repeatable fabrication of a parabolic shape on diamond waveguides may still be difficult relative to high-fidelity patterning of SiN, we focus on pitch-defect cavity designs for the remainder of this paper. However, for other combinations of materials and emitters, width defect cavities may be more practical. For example, there are methods for fabricating periodic grating lines without pitch tapers via photolithography below the diffraction limit such as interference lithography.[46]

Figure 2(a) illustrates important design parameters for the pitch-defect cavity, while Figs. 2(b)–2(d) show a numerically calculated mode (Ansys Lumerical) for an exemplary hybrid cavity geometry at 619.5 nm to match the SnV ZPL wavelength. We also calculated the dispersion curves (MIT Photonic Bands) for the diamond waveguide and the SiN/air grating individually, plotted in Fig. 2(e). Throughout all subsequent numerical simulations, we use the following refractive indices for air $n_{\text{air}} = 1$, SiN $n_{\text{SiN}} = 1.95$, and diamond $n_{\text{dmd}} = 2.42$.

The dispersion curves in Fig. 2(e) give initial guidance and insight into how the hybrid cavity is formed. First, the cavity frequency of interest must lie in the bandgap of the SiN/air mirror regions but outside the bandgap in the pitch-defect region. This is easily performed by adjusting the pitch $a1$ appropriately. Second, the diamond waveguide mode must couple efficiently to the underlying

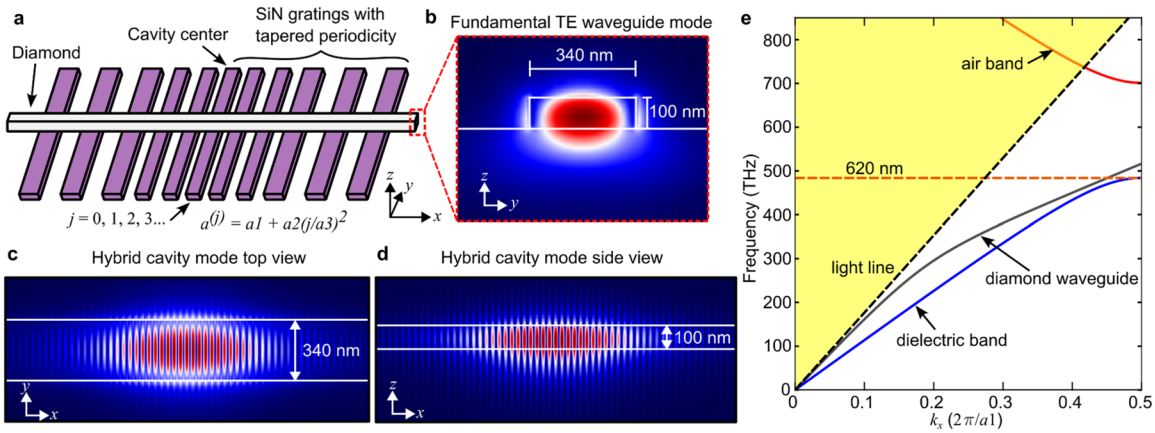

FIG. 2. Design of the pitch-defect hybrid cavity. (a) The pitch-defect hybrid cavity is composed of a diamond waveguide placed on top of a dielectric (SiN) grating with a parabolic-tapered periodicity from the center of the cavity. (b) Numerical calculation of the fundamental TE diamond–SiN hybrid optical mode. (c) and (d) Numerical calculations of the hybrid cavity mode seen from the top and side views, respectively. (e) Individual band diagrams for the SiN periodic grating structure (labeled dielectric and air bands) and the diamond waveguide dispersion (labeled diamond waveguide) for the central pitch of an exemplary hybrid cavity with $a1$ = 170 nm, $a5$ = 0.5, $b1$ = 340 nm, and $b4$ = 100 nm.

grating structure, suggesting spatial overlap and phase matching conditions. Specifically, the approximate phase matching condition should be satisfied,

$$n_{eff,dmd} \approx (1 - a_5)n_{air} + a_5 n_{SiN}. \quad (2)$$

As the refractive index of diamond is much larger than that of SiN and air, making the diamond waveguide thin enables both better phase matching and spatial overlap due to a larger vertical evanescent field. We settle on a diamond thickness of $b4$ = 100 nm and widths $b1$ around 300–400 nm, which satisfy the aforementioned requirements while being within reasonable fabrication limits.[37,47]

While the band diagrams [Fig. 2(e)] are a good starting point, the real optical mode is hybridized between the diamond and underlying dielectric grating. We calculate the hybrid mode bandgap (Fig. 3) using a fully 3D finite-difference time-domain wave propagation simulation (ANSYS Lumerical), which nominally follows the bands calculated in Fig. 2(e). These hybrid mode simulations fully account for the phase matching and mode overlap conditions required to form a usable cavity.

With an understanding of the hybrid mode bandgap, we proceed to design a high-Q quantum optical cavity. Figure 4(a) shows the simulation where the cavity mode is found by sweeping a TE dipole source frequency while monitoring each frequency's field decay in time. The cavity mode frequency and quality factor are extracted and plotted with respect to the diamond width [Figs. 4(b) and 4(c)] for different grating periodicities ($a1$). The simulated unloaded quality factor for these cavities generally ranges from 10^5 to 10^6 with relatively little sensitivity to different diamond geometries. Therefore, we observe that, for an already fabricated grating mirror geometry, we can readily tune the cavity mode over tens of nanometers by selectively stamping a diamond waveguide of appropriate width. This can be useful for cavity mode adjustment, as different diamond waveguides may be placed onto the SiN and replaced with a waveguide of different geometry if needed, enabling coarse tuning of the cavity without resorting to new fabrication.

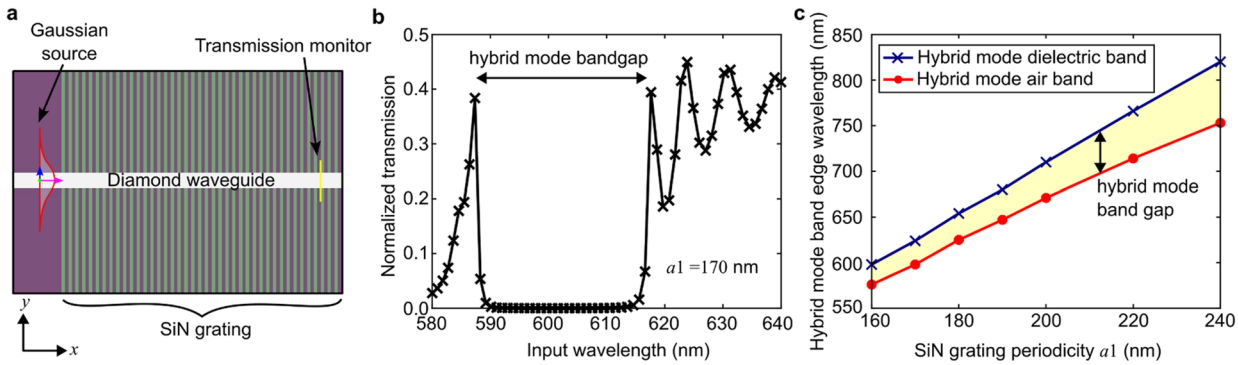

FIG. 3. Simulations of the hybrid optical mode bandgap. (a) Diagram of Gaussian propagation simulations of the full 3D hybrid geometry for variable SiN periodicity and diamond waveguide dimensions of $b1$ = 340 nm wide, $b4$ = 100 nm high. (b) Normalized transmission plot of the hybrid diamond–SiN propagation with $a1$ = 170 nm showing the bandgap as a function of the input wavelength, which accounts for the bandgap of the periodic structure, the diamond waveguide dispersion, and the evanescent coupling between the two materials. (c) Wavelength band edges extracted from additional transmission simulations. The air and dielectric bands are plotted for various SiN periodicities.

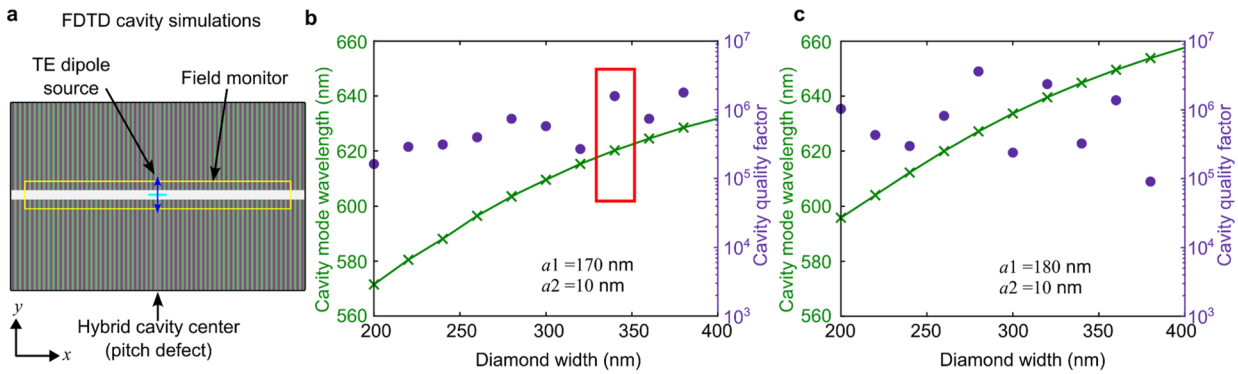

FIG. 4. Cavity mode dependence on diamond waveguide width with a fixed SiN grating geometry. (a) Diagram of the hybrid cavity simulation with a TE point dipole source and surrounding E-field monitor. (b) and (c) Cavity mode wavelength and quality factor vs diamond waveguide width for a pitch-defect design with $a1$ = 170 nm and $a1$ = 180 nm, respectively. The other cavity parameters are $a2$ = 10 nm, $a3$ = 20 periods, $a4$ = 150 nm, $a5$ = 0.5, and $b4$ = 100 nm. The red rectangle in (b) highlights the geometric parameters used for the simulations in Figs. 2, 3, 5, and 6.

TABLE II. List of geometries with Q optimized cavity modes.

Parameter	Geometry 1	Geometry 2	Geometry 3
$a1$	180 nm	180 nm	170 nm
$a2$	10 nm	10 nm	10 nm
$a3$	20	20	20
$a4$	150 nm	150 nm	150 nm
$a5$	0.5	0.5	0.5
$b1$	310 nm	400 nm	340 nm
$b2$	0	0	0
$b3$	0	0	0
$b4$	100 nm	100 nm	100 nm
Cavity mode	636.5 nm	657.7 nm	619.5 nm
Q	5.77×10^7	1.50×10^6	3.95×10^5
V	4.54×10^{-20} m^3	5.31×10^{-20} m^3	4.50×10^{-20} m^3
n_{eff}	1.81	1.85	1.852
$V_{norm}\ (\lambda/n_{eff})^3$	1.04	1.19	1.2

Previous work on this PIC platform has shown adiabatically tapered SiN waveguides robust to repeated placements of different diamond chiplets for on-chip photon readout.

A summary of selected simulation geometries with quality factor and mode volume is listed in Table II, with cavity mode wavelengths located around the NV ZPL and SnV ZPL. We note that simulated quality factors are generally accurate only to within an order of magnitude due to fitting the gradual exponential decay calculated from the field monitors. The extracted mode volumes of the hybrid cavity are only slightly larger than monolithic diamond nanobeam PhC cavities,[9,12,39] while offering repeatable and flexible cavity construction.

In order to complete the hybrid cavity design, we note that simply maximizing the intrinsic Q is not sufficient for quantum operations. As previously mentioned, a high collection efficiency η_2 is needed. We investigate the trade-off between outcoupling and intrinsic Q by calculating additional cavity geometries with variable mirror periods on one side of the cavity. With a simulation setup as in Fig. 4(a), we vary the number of mirror periods on one side of the cavity to find how the new "loaded" quality factor Q varies with η_2. We note that the number of mirror periods does not include the existing taper region from the central pitch of the SiN lines to the section where the mirror pitch starts. For example, a simulation with parameters $a1$ = 170 nm, $a2$ = 10 nm, $a3$ = 20 periods, and 0 mirror periods on one side would still have on that side 20 SiN lines tapering from 170 nm out to 180 nm, where the mirror region would then otherwise begin in a Q-optimized cavity. The number of mirror periods dictates the reflectivity at each side of the cavity.

For these simulations, we also introduce some fabrication non-idealities for comparison to give a better sense of how real devices behave. Specifically, we assume two orders of magnitude lower Q than calculated (this presumes additional losses purely due to scattering and absorption effects) and only 50% alignment of the color center dipole and cavity-mode electric field. We label these values with the (fab) designation in the plots.

We make these quality factor assumptions based on prior work fabricating monolithic diamond cavities, where the as-fabricated quality factor ranges from approximately one to three orders of magnitude worse than the theoretical calculation in simulation.[9,22,39,48] We model a "typical" scenario where the as-fabricated Q is brought down to match previous experimental results (decreased by two orders of magnitude from our simulated value) to show that in such a situation, we can still achieve the necessary Purcell enhancement for high collection efficiency of photons necessary for entanglement protocols.

The NV- and group-IV color center dipole orientations are along the [111] (or an equivalent) axis, and the diamond slab used for fabrication has a [001]-oriented top surface. The fabrication of the diamond chiplets is performed to orient the TE mode of the cavity in the [110] direction. The angle between the emitter and TE cavity mode orientation is then 35.26°. The Purcell effect depends on the angular overlap of the cavity mode and emitter dipole; therefore, assuming the emitter dipole is spatially located at the maximum electric field value of the cavity, the fraction of maximum Purcell enhancement compared to perfectly aligned dipoles is given by cos(35.26°) = 0.816, which is larger than our 50% approximation

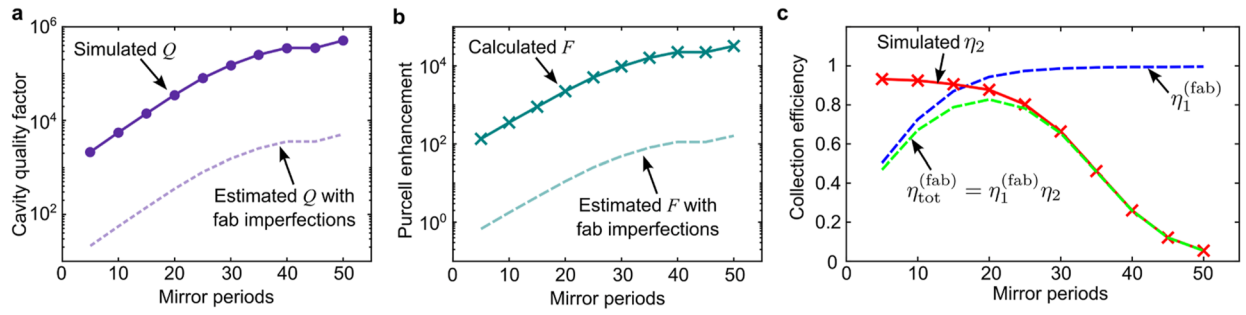

FIG. 5. Optimizing η_{tot} for outcoupling of the hybrid cavity to a photonic integrated circuit. Simulations were performed for a dielectric pitch-defect cavity mode at 619.5 nm, with geometric parameters $a1$ = 170 nm, $a2$ = 10 nm, $a3$ = 20 periods, $a4$ = 150 nm, and $a5$ = 0.5. $b1$ = 340 nm, $b4$ = 100 nm. (a) Simulated Q as the number of mirror periods on the photon collection side is varied. More mirror periods generally lead to higher Q. An estimated, lower Q due to fabrication imperfections is also plotted. (b) Calculated Purcell factor F based on the simulated Q, including an estimated, lower F due to fabrication imperfections. (c) Coupling efficiencies $\eta_1^{(fab)}$, η_2, and $\eta_{tot}(fab)$, which take into account the lower Q and F due to fabrication imperfections. There is an optimal mirror period number that balances high collection efficiency via the waveguide while maintaining a high Purcell factor of the cavity.

used in these calculations. Achieving perfect spatial alignment of the emitter with the maximum electric field is practically difficult as well due to the stochastic process by which defects are typically generated in diamond. Our hybrid system has the advantage that the position of the diamond waveguide can be adjusted to better align a specific emitter to the center of the cavity without changing the geometry of the cavity due to translation invariance along the length of the diamond waveguide.

Figure 5 shows simulations of the 619.5 nm cavity mode Q, Purcell factor F, and total collection efficiency η_{tot} as the number of mirror periods is varied. We find that in an idealized high-Q regime, the Purcell factor likewise remains high such that η_1 is always efficient and close to 1. Here the total collection efficiency η_{tot} is simply dominated by the output collection η_2, preferring low mirror period designs. However, in as-fabricated cavities that typically operate with much lower Q and F, $\eta_1(fab)$ decreases rapidly as the number of mirror periods becomes too low [Fig. 5(c)]. Therefore, there is an optimal number of mirror periods that avoids low reflectivity causing Q and hence F to lose its effectiveness in maintaining efficient η_1 but still allows efficient total outcoupling η_{tot}. We achieve an optimal design with $F = 11$ (with fabrication-imperfect Q) and $\eta_{tot} = 0.828$ at about 20 mirror periods. Once light propagates beyond the mirror region of the cavity, the diamond can be efficiently coupled to underlying SiN waveguides on an active photonics platform. Previous results have shown that optimized coupling between a tapered diamond waveguide and an underlying tapered SiN waveguide can reach up to 0.95.[49] When combining this with SnVs high internal quantum efficiency of 0.8,[42] the total photon collection efficiency from the cavity to the SiN waveguide is $\eta \approx 0.629$. This is well above collection efficiencies previously considered for calculating the percolation threshold of cluster states for quantum computing.[50]

There are additional techniques that could be implemented to make outcoupling alignment simpler as well, such as with angled interconnects.[51] We note that vertical free-space collection designs are also possible (see supplementary material, Sec. 2).

HYBRID CAVITY AND EMITTER TUNING WITH PIEZOELECTRIC ACTUATION

While we presented an optical cavity with flexible characteristics, a further advantage of the hybrid design is the ability to include CMOS-fabricated fine tuning of the underlying dielectric-grating during hybrid cavity generation. This can help correct for geometric variation due to fabrication imperfections that shift the cavity mode away from the theoretically modeled frequency. (We analyze how variation in the grating fill factor can shift the cavity

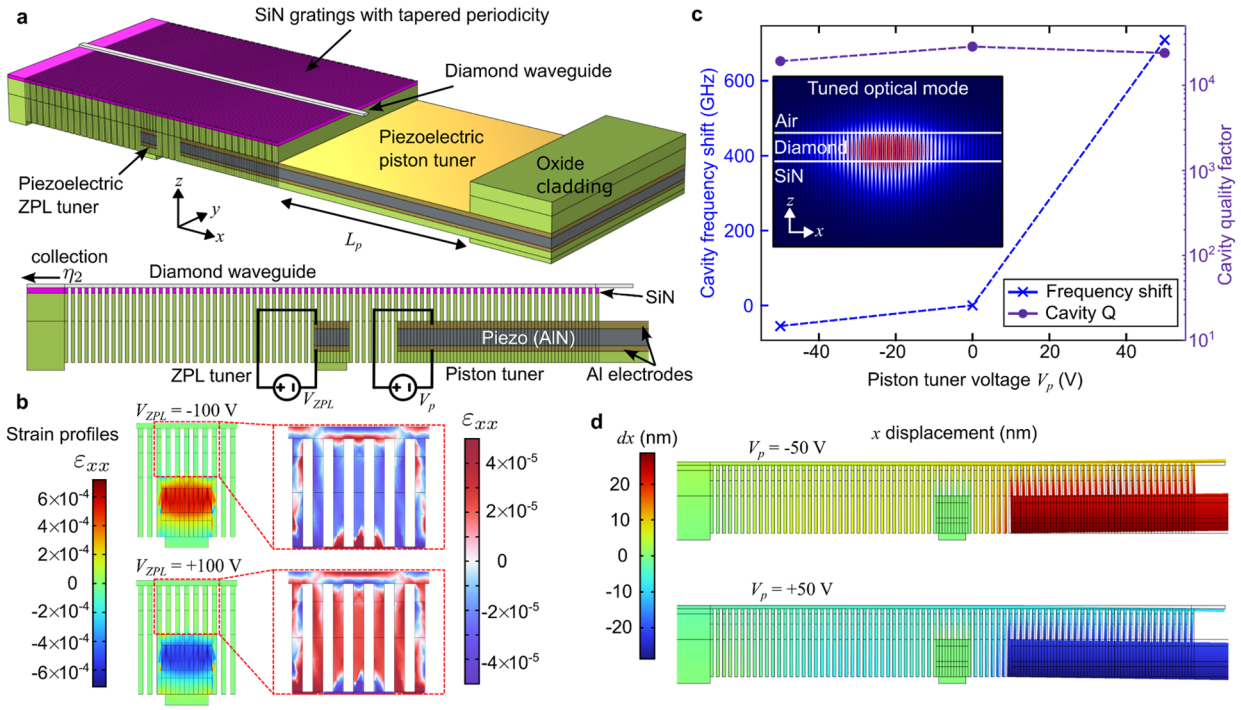

FIG. 6. Integrated piezoelectric tuning of the hybrid cavity mode. (a) Cavity strain tuning platform schematic showing the geometry of the hybrid cavity coupled to two independent piezoelectric tuners: the ZPL tuner and the piston tuner. The voltage V_{ZPL} controls the ZPL tuner, and V_p controls the piston tuner. Light green = oxide cladding, yellow = aluminum, dark gray = aluminum nitride/piezoelectric tuner, purple = silicon nitride grating, light gray waveguide = diamond. (b) Strain profile of ε_{xx} when the ZPL tuner voltage is ±100 V, showing strain propagating up to the diamond waveguide to tune the emitter's ZPL wavelength. (c) Cavity mode (inset: E-field magnitude at $V_p = 0$, XZ cross section) tuning when applying voltage to the piston tuner, tuning up to 760 GHz from −50 to 50 V while preserving quality factor. (d) Total x-displacement of the hybrid cavity when $V_p = \pm 50$ V is applied to the piston cantilever.

mode in supplementary material, Sec. 3.) This tunability allows robust alignment of different color centers in different cavities all to a single frequency.

We propose a tuning method by attaching our hybrid cavity to a piezoelectric-piston body consisting of the same layer stack as our previously reported cryogenically compatible photonics technology,[38] shown in Fig. 6. This chip stack is composed of a piezoelectric aluminum nitride (AlN) layer sandwiched between two aluminum (Al) electrodes where applied voltage causes deformations in the AlN and thereby the entire cantilever. The electrodes are controlled by underlying routing metal connected to the electrodes by tungsten vias. An underlying amorphous silicon (aSi) layer is etched away by a post-fabrication xenon difluoride gas, creating the free floating cantilever with a bottom layer of silicon dioxide.

To calculate cavity mode tuning, we first modify the 619.5 nm cavity mode design to have only 20 mirror periods on each side, in addition to the a3 = 20 period taper region from the center of the cavity [Fig. 6(a)]. The taper sections are etched through and connected only at the ends in a snake-like pattern, thereby reducing the overall mechanical rigidity of the cavity region. One side of the cavity is clamped with the mirror section lines connected at both ends to each other to maintain their rigidity. This causes a concentration of any geometric deformations toward the center of the cavity. The other side is attached to a free-floating cantilever consisting of the piezoelectric layer (AlN) and electrodes (Al) with a layer of silicon dioxide at the bottom. The mirror section on this side rests on top of the cantilever, and the etch of the SiN lines stops at the top Al surface. The cantilever piston will readily push or pull against the cavity depending on the polarity of the applied voltage. By design, the generated strain will highly concentrate[52] in the cavity region due to the large difference between the effective mechanical compliance of the cantilever piston and the cavity mirror regions. To add a second tuning degree of freedom, an additional "ZPL" piezo-actuator is placed underneath the center of the cavity. By applying ±100 V to this piezo, additional strain is generated in the diamond locally near the emitter of interest. The ZPL tuner allows us to control the color center's ZPL wavelength independently of the cavity piston tuner to better align with the optical cavity resonance.

We investigate the hybrid cavity tuning using finite-element (COMSOL) simulations, depicted in Fig. 6(a). We first perform COMSOL simulations for a combination of piston (−50, 0, 50 V) and ZPL piezo (−100, 0, 100 V) voltages to strain the cavity. The re-meshed, deformed geometry and strain values are exported from COMSOL directly into Ansys Lumerical to accurately capture moving boundary contributions to the cavity mode shifts. For the strain-optic effects, we converted volume-averaged strains [Fig. 6(b)] to material index shifts in the deformed geometry, discretized into several regions. However, we found the strain-optic effect had an overall negligible effect on the cavity tuning (only <10 GHz shift, more details in supplementary material, Sec. 4). The resulting cavity mode shifts based primarily on moving material boundaries are shown in Fig. 6(c). We find that by applying voltages in the range of −50 to 50 V (readily accessible voltages on our platform), we can tune the cavity mode by ~760 GHz relative to the unperturbed mode. Figure 6(d) shows the deformations induced by the piezoelectric piston at these voltages.

In this design, the ZPL of a color center in diamond will also be tuned by the strain field, whose effect will somewhat vary depending on the exact location in the cavity. Based on experimental strain tuning of SnVs with a ZPL near 619.5 nm of ~0.5 PHz/strain,[47] our max strain values using the center ZPL piezo alone are on the order of 10^{-5} [Fig. 6(b)] corresponding to a ZPL tuning of ~5 GHz. Given an implanted ensemble of SnVs with a transform-limited linewidth of ~30 MHz, we can readily tune across dozens of SnVs to isolate a single emitter within the cavity. We note there is additional tuning of the ZPL due to the strain induced by the piston cantilever, on the order of 10^{-4} corresponding to a ~50 GHz shift for the ZPL. However, because the cavity mode shift is an order of magnitude larger, it is possible to find a pair of tuning voltages for the piston and ZPL tuner (fine adjustment) that align the cavity mode and the ZPL wavelengths. Finally, since the strain due to the piston cantilever is approximately one order of magnitude higher than that due to the ZPL piezo, we found the cavity tuning resulting strictly from the ZPL piezo was below the accuracy threshold of the optical simulation.

DISCUSSION

The hybrid cavity provides several inherent advantages in terms of fabrication reliability and scalability compared to existing approaches. Our approach transfers the complexity of high-resolution fabrication into mature CMOS materials such as SiN or SiO_2, enabling integration with existing complex photonic layer stacks[38] while increasing yield. These features would enable both direct piezoelectric tuning of the cavity (faster and more flexible than existing capacitive,[53,54] laser tuning,[55,56] or gas tuning methods)[9,48] as well as photon collection into reconfigurable photonic circuits such as integrated switches and multiport interferometers.[57] On the diamond material side, the geometry of the stamped waveguide may be post-selected for additional reliability when targeting a specific wavelength, such as 620 nm for SnV in diamond. Fabricating rectangular diamond waveguides is also a simpler process compared to fabricating fine-featured nanobeams or PhC cavities in the diamond itself. In addition, the color centers may be placed further from diamond etched surfaces in the waveguide compared to a PhC, thereby decreasing potential effects of nearby surface states to cause defect ionization or spectral diffusion.[58] High quality fabrication of diamond waveguide microchiplets has already been demonstrated in prior works[37] and shown to couple efficiently to underlying PICs, with modeling showing up to 95% coupling efficiency via adiabatic tapers.[49] Experimental readout of color center photons via the SiN waveguides in the underlying PIC indicates good physical contact between the two materials.

To realize our device experimentally, we may leverage our CMOS-fabricated photonics platform[38] by designing both the ZPL piezo and the piston tuner around a prepared film of SiN. We can utilize back-end-of-line processes such as electron beam lithography, focused ion beam, or deep UV lithography[59,60] to write the desired pitch-defect lines into the SiN. Once the SiN component is patterned and released, we can directly pick and place with a PDMS stamp to transfer a separately fabricated diamond QMC onto the SiN pattern to complete the hybrid cavity. The highly reflective end of the cavity is attached to the piston cantilever, whereas the end designed for photon output can have an array of underlying tapered SiN waveguides[47] where the output photons through the diamond waveguide can be coupled for further photon routing, entanglement,

and detection schemes. The pick and stamp process may be scaled by potentially designing our wafer stack with a lock and release method previously demonstrated for large-scale heterogeneous integration of diamond QMC arrays on a CMOS platform.[61]

SUPPLEMENTARY MATERIAL

The supplementary material includes Ansys Lumerical simulation details, cavity designs for free space collection, cavity mode shift calculations due to potential variations in fabrication etch duty cycle, and details for calculating the strain-optic effect in cavity tuning 3D simulations.

ACKNOWLEDGMENTS

M.D. and A.S.G. acknowledge Y. H. Wen, G. Clark, D. A. Golter, K. J. Palm, and A. Khaykin for helpful technical discussions. M.D. and A.S.G. acknowledge T. E. Espedal for providing auxiliary hybrid cavity simulations. MITRE Quantum Moonshot Project; DARPA ONISQ program; Brookhaven National Laboratory supported by U.S. Department of Energy, Office of Basic Energy Sciences, under Contract No. DE-SC0012704; NSF RAISE TAQS program; Center for Integrated Nanotechnologies, an Office of Science User Facility operated by the U.S. Department of Energy Office of Science.

AUTHOR DECLARATIONS

Conflict of Interest

D.E. is a scientific advisor to and holds shares in QuEra Computing, Qunett, and Axiomatic_AI. The other authors declare no conflict of interest.

Author Contributions

A.S.G. and M.D. are contributed equally to this work.

Andrew S. Greenspon: Conceptualization (equal); Data curation (equal); Investigation (equal); Methodology (equal); Validation (equal); Writing – original draft (equal); Writing – review & editing (equal). **Mark Dong**: Conceptualization (equal); Data curation (equal); Investigation (equal); Methodology (equal); Validation (equal); Writing – original draft (equal); Writing – review & editing (equal). **Ian Christen**: Conceptualization (equal); Investigation (supporting); Methodology (supporting); Writing – original draft (supporting). **Gerald Gilbert**: Funding acquisition (equal); Project administration (supporting); Writing – review & editing (supporting). **Matt Eichenfield**: Project administration (supporting); Writing – review & editing (supporting). **Dirk Englund**: Conceptualization (lead); Project administration (lead); Writing – review & editing (supporting).

DATA AVAILABILITY

The data underlying the results presented in this paper are not publicly available at this time but may be obtained from the corresponding author upon reasonable request.

REFERENCES

[1] M. Li, J. Ling, Y. He, U. A. Javid, S. Xue, and Q. Lin, "Lithium niobate photonic-crystal electro-optic modulator," Nat. Commun. **11**, 4123 (2020).
[2] A. C. Liapis, B. Gao, M. R. Siddiqui, Z. Shi, and R. W. Boyd, "On-chip spectroscopy with thermally tuned high-Q photonic crystal cavities," Appl. Phys. Lett. **108**, 021105 (2016).
[3] Y. Long, J. Xia, Y. Zhang, J. Dong, and J. Wang, "Photonic crystal nanocavity assisted rejection ratio tunable notch microwave photonic filter," Sci. Rep. **7**, 40223 (2017).
[4] P. Yu, H. Qiu, T. Dai, R. Cheng, B. Lian, W. Li, H. Yu, and J. Yang, "Ultracompact channel add-drop filter based on single multimode nanobeam photonic crystal cavity," J. Lightwave Technol. **39**, 162–166 (2021).
[5] Y. Zhang, P. Liu, S. Zhang, W. Liu, J. Chen, and Y. Shi, "High sensitivity temperature sensor based on cascaded silicon photonic crystal nanobeam cavities," Opt. Express **24**, 23037–23043 (2016).
[6] Y. Liu and H. W. M. Salemink, "Photonic crystal-based all-optical on-chip sensor," Opt. Express **20**, 19912–19920 (2012).
[7] G. Marty, S. Combrié, F. Raineri, and A. De Rossi, "Photonic crystal optical parametric oscillator," Nat. Photonics **15**, 53–58 (2021).
[8] K. Hennessy, A. Badolato, M. Winger, D. Gerace, M. Atatüre, S. Gulde, S. Fält, E. L. Hu, and A. Imamoğlu, "Quantum nature of a strongly coupled single quantum dot–cavity system," Nature **445**, 896–899 (2007).
[9] A. E. Rugar, S. Aghaeimeibodi, D. Riedel, C. Dory, H. Lu, P. J. McQuade, Z.-X. Shen, N. A. Melosh, and J. Vučković, "Quantum photonic interface for tin-vacancy centers in diamond," Phys. Rev. X **11**, 031021 (2021).
[10] J. L. Zhang, S. Sun, M. J. Burek, C. Dory, Y.-K. Tzeng, K. A. Fischer, Y. Kelaita, K. G. Lagoudakis, M. Radulaski, Z.-X. Shen, N. A. Melosh, S. Chu, M. Lončar, and J. Vučković, "Strongly cavity-enhanced spontaneous emission from silicon-vacancy centers in diamond," Nano Lett. **18**, 1360–1365 (2018).
[11] B. J. M. Hausmann, B. J. Shields, Q. Quan, Y. Chu, N. P. de Leon, R. Evans, M. J. Burek, A. S. Zibrov, M. Markham, D. J. Twitchen, H. Park, M. D. Lukin, and M. Loncăr, "Coupling of NV centers to photonic crystal nanobeams in diamond," Nano Lett. **13**, 5791–5796 (2013).
[12] K. Kuruma, B. Pingault, C. Chia, D. Renaud, P. Hoffmann, S. Iwamoto, C. Ronning, and M. Lončar, "Coupling of a single tin-vacancy center to a photonic crystal cavity in diamond," Appl. Phys. Lett. **118**, 230601 (2021).
[13] A. L. Crook, C. P. Anderson, K. C. Miao, A. Bourassa, H. Lee, S. L. Bayliss, D. O. Bracher, X. Zhang, H. Abe, T. Ohshima, E. L. Hu, and D. D. Awschalom, "Purcell enhancement of a single silicon carbide color center with coherent spin control," Nano Lett. **20**, 3427–3434 (2020).
[14] Ł. Dusanowski, D. Köck, C. Schneider, and S. Höfling, "On-chip Hong–Ou–Mandel interference from separate quantum dot emitters in an integrated circuit," ACS Photonics **10**, 2941–2947 (2023).
[15] C. Papon, Y. Wang, R. Uppu, S. Scholz, A. D. Wieck, A. Ludwig, P. Lodahl, and L. Midolo, "Independent operation of two waveguide-integrated quantum emitters," Phys. Rev. Appl. **19**, L061003 (2023).
[16] T. Zhong, J. M. Kindem, E. Miyazono, and A. Faraon, "Nanophotonic coherent light–matter interfaces based on rare-earth-doped crystals," Nat. Commun. **6**, 8206 (2015).
[17] T. Zhong, J. M. Kindem, J. G. Bartholomew, J. Rochman, I. Craiciu, V. Verma, S. W. Nam, F. Marsili, M. D. Shaw, A. D. Beyer, and A. Faraon, "Optically addressing single rare-earth ions in a nanophotonic cavity," Phys. Rev. Lett. **121**, 183603 (2018).
[18] J. Arjona Martínez, R. A. Parker, K. C. Chen, C. M. Purser, L. Li, C. P. Michaels, A. M. Stramma, R. Debroux, I. B. Harris, M. Hayhurst Appel, E. C. Nichols, M. E. Trusheim, D. A. Gangloff, D. Englund, and M. Atatüre, "Photonic indistinguishability of the tin-vacancy center in nanostructured diamond," Phys. Rev. Lett. **129**, 173603 (2022).
[19] M. J. Burek, Y. Chu, M. S. Z. Liddy, P. Patel, J. Rochman, S. Meesala, W. Hong, Q. Quan, M. D. Lukin, and M. Lončar, "High quality-factor optical nanocavities in bulk single-crystal diamond," Nat. Commun. **5**, 5718 (2014).
[20] E. M. Purcell, "Proceedings of the American physical society," Phys. Rev. **69**, 674 (1946).

[21] A. Faraon, C. Santori, Z. Huang, V. M. Acosta, and R. G. Beausoleil, "Coupling of nitrogen-vacancy centers to photonic crystal cavities in monocrystalline diamond," Phys. Rev. Lett. **109**, 033604 (2012).
[22] S. W. Ding, M. Haas, X. Guo, K. Kuruma, C. Jin, Z. Li, D. D. Awschalom, N. Delegan, F. J. Heremans, A. A. High, and M. Loncar, "High-Q cavity interface for color centers in thin film diamond," Nat. Commun. **15**, 6358 (2024).
[23] S. Cui, X. Zhang, T.-L. Liu, J. Lee, D. Bracher, K. Ohno, D. Awschalom, and E. L. Hu, "Hybrid plasmonic photonic crystal cavity for enhancing emission from near-surface nitrogen vacancy centers in diamond," ACS Photonics **2**, 465–469 (2015).
[24] P. E. Barclay, K.-M. C. Fu, C. Santori, A. Faraon, and R. G. Beausoleil, "Hybrid nanocavity resonant enhancement of color center emission in diamond," Phys. Rev. X **1**, 011007 (2011).
[25] M. Gould, E. R. Schmidgall, S. Dadgostar, F. Hatami, and K.-M. C. Fu, "Efficient extraction of zero-phonon-line photons from single nitrogen-vacancy centers in an integrated GaP-on-diamond platform," Phys. Rev. Appl. **6**, 011001 (2016).
[26] S. Chakravarthi, N. S. Yama, A. Abulnaga, D. Huang, C. Pederson, K. Hestroffer, F. Hatami, N. P. de Leon, and K.-M. C. Fu, "Hybrid integration of GaP photonic crystal cavities with silicon-vacancy centers in diamond by stamp-transfer," Nano Lett. **23**, 3708–3715 (2023).
[27] M. H. Rahaman, C.-M. Lee, M. A. Buyukkaya, Y. Zhao, and E. Waks, "Hybrid Si-GaAs photonic crystal cavity for lasing and bistability," Opt. Express **31**, 37574–37582 (2023).
[28] S. Mauthe, P. Tiwari, M. Scherrer, D. Caimi, M. Sousa, H. Schmid, K. E. Moselund, and N. Vico Triviño, "Hybrid III–V silicon photonic crystal cavity emitting at telecom wavelengths," Nano Lett. **20**, 8768–8772 (2020).
[29] G. Marty, S. Combrié, A. De Rossi, and F. Raineri, "Hybrid InGaP nanobeam on silicon photonics for efficient four wave mixing," APL Photonics **4**, 120801 (2019).
[30] S. Cui, A. S. Greenspon, K. Ohno, B. A. Myers, A. C. B. Jayich, D. D. Awschalom, and E. L. Hu, "Reduced plasma-induced damage to near-surface nitrogen-vacancy centers in diamond," Nano Lett. **15**, 2887–2891 (2015).
[31] B. L. Dwyer, L. V. H. Rodgers, E. K. Urbach, D. Bluvstein, S. Sangtawesin, H. Zhou, Y. Nassab, M. Fitzpatrick, Z. Yuan, K. De Greve, E. L. Peterson, H. Knowles, T. Sumarac, J.-P. Chou, A. Gali, V. V. Dobrovitski, M. D. Lukin, and N. P. De Leon, "Probing spin dynamics on diamond surfaces using a single quantum sensor," PRX Quantum **3**, 040328 (2022).
[32] B. A. Myers, A. Das, M. C. Dartiailh, K. Ohno, D. D. Awschalom, and A. C. Bleszynski Jayich, "Probing surface noise with depth-calibrated spins in diamond," Phys. Rev. Lett. **113**, 027602 (2014).
[33] Z.-H. Zhang, J. A. Zuber, L. V. H. Rodgers, X. Gui, P. Stevenson, M. Li, M. Batzer, M. L. Grimau Puigibert, B. J. Shields, A. M. Edmonds, N. Palmer, M. L. Markham, R. J. Cava, P. Maletinsky, and N. P. de Leon, "Neutral silicon vacancy centers in undoped diamond via surface control," Phys. Rev. Lett. **130**, 166902 (2023).
[34] J. Görlitz, D. Herrmann, P. Fuchs, T. Iwasaki, T. Taniguchi, D. Rogalla, D. Hardeman, P.-O. Colard, M. Markham, M. Hatano, and C. Becher, "Coherence of a charge stabilised tin-vacancy spin in diamond," npj Quantum Inf. **8**, 45 (2022).
[35] B. A. Myers, A. Ariyaratne, and A. C. B. Jayich, "Double-quantum spin-relaxation limits to coherence of near-surface nitrogen-vacancy centers," Phys. Rev. Lett. **118**, 197201 (2017).
[36] S. Sangtawesin, B. L. Dwyer, S. Srinivasan, J. J. Allred, L. V. H. Rodgers, K. De Greve, A. Stacey, N. Dontschuk, K. M. O'Donnell, D. Hu, D. A. Evans, C. Jaye, D. A. Fischer, M. L. Markham, D. J. Twitchen, H. Park, M. D. Lukin, and N. P. de Leon, "Origins of diamond surface noise probed by correlating single-spin measurements with surface spectroscopy," Phys. Rev. X **9**, 031052 (2019).
[37] N. H. Wan, T.-J. Lu, K. C. Chen, M. P. Walsh, M. E. Trusheim, L. De Santis, E. A. Bersin, I. B. Harris, S. L. Mouradian, I. R. Christen, E. S. Bielejec, and D. Englund, "Large-scale integration of artificial atoms in hybrid photonic circuits," Nature **583**, 226–231 (2020).
[38] M. Dong, G. Clark, A. J. Leenheer, M. Zimmermann, D. Dominguez, A. J. Menssen, D. Heim, G. Gilbert, D. Englund, and M. Eichenfield, "High-speed programmable photonic circuits in a cryogenically compatible, visible–near-infrared 200 mm CMOS architecture," Nat. Photonics **16**, 59–65 (2021).
[39] S. Mouradian, N. H. Wan, T. Schröder, and D. Englund, "Rectangular photonic crystal nanobeam cavities in bulk diamond," Appl. Phys. Lett. **111**, 021103 (2017).
[40] H. Raniwala, I. Christen, K. C. Chen, D. Starling, and D. Englund, "Integrating nearly-indistinguishable quantum emitters onto a photonic interposer," in *CLEO 2023* (Optica Publishing Group, 2023), pp. M1H–M3.
[41] Q. Quan and M. Loncar, "Deterministic design of wavelength scale, ultra-high Q photonic crystal nanobeam cavities," Opt. Express **19**, 18529–18542 (2011).
[42] T. Iwasaki, Y. Miyamoto, T. Taniguchi, P. Siyushev, M. H. Metsch, F. Jelezko, and M. Hatano, "Tin-vacancy quantum emitters in diamond," Phys. Rev. Lett. **119**, 253601 (2017).
[43] J. Görlitz, D. Herrmann, G. Thiering, P. Fuchs, M. Gandil, T. Iwasaki, T. Taniguchi, M. Kieschnick, J. Meijer, M. Hatano, A. Gali, and C. Becher, "Spectroscopic investigations of negatively charged tin-vacancy centres in diamond," New J. Phys. **22**, 013048 (2020).
[44] Y. Duan, K. C. Chen, D. R. Englund, and M. E. Trusheim, "A vertically-loaded diamond microdisk resonator spin-photon interface," Opt. Express **29**, 43082 (2021).
[45] L. Li, H. Choi, M. Heuck, and D. Englund, "Field-based design of a resonant dielectric antenna for coherent spin-photon interfaces," Opt. Express **29**, 16469–16476 (2021).
[46] C. Lu and R. H. Lipson, "Interference lithography: A powerful tool for fabricating periodic structures," Laser Photonics Rev. **4**, 568–580 (2010).
[47] G. Clark, H. Raniwala, M. Koppa, K. Chen, A. Leenheer, M. Zimmermann, M. Dong, L. Li, Y. H. Wen, D. Dominguez, M. Trusheim, G. Gilbert, M. Eichenfield, and D. Englund, "Nanoelectromechanical control of spin–photon interfaces in a hybrid quantum system on chip," Nano Lett. **24**, 1316–1323 (2024).
[48] K. C. Chen, I. Christen, H. Raniwala, M. Colangelo, L. De Santis, K. Shtyrkova, D. Starling, R. Murphy, L. Li, K. Berggren, P. B. Dixon, M. Trusheim, and D. Englund, "A scalable cavity-based spin–photon interface in a photonic integrated circuit," Opt. Quantum **2**, 124 (2024).
[49] D. A. Golter, G. Clark, T. El Dandachi, S. Krastanov, A. J. Leenheer, N. H. Wan, H. Raniwala, M. Zimmermann, M. Dong, K. C. Chen, L. Li, M. Eichenfield, G. Gilbert, and D. Englund, "Selective and scalable control of spin quantum memories in a photonic circuit," Nano Lett. **23**, 7852–7858 (2023).
[50] H. Choi, M. Pant, S. Guha, and D. Englund, "Percolation-based architecture for cluster state creation using photon-mediated entanglement between atomic memories," npj Quantum Inf. **5**, 104–107 (2019).
[51] S. Bandyopadhyay and D. Englund, "Alignment-free photonic interconnects," arXiv:2110.12851 [physics.app-ph] (2021).
[52] S. P. Timoshenko and J. N. Goodier, *Theory of Elasticity*, Engineering Societies Monographs, 3rd ed. (McGraw-Hill, 1970).
[53] S. Maity, L. Shao, Y.-I. Sohn, S. Meesala, B. Machielse, E. Bielejec, M. Markham, and M. Lončar, "Spectral alignment of single-photon emitters in diamond using strain gradient," Phys. Rev. Appl. **10**, 024050 (2018).
[54] S. Meesala, Y.-I. Sohn, B. Pingault, L. Shao, H. A. Atikian, J. Holzgrafe, M. Gündoğan, C. Stavrakas, A. Sipahigil, C. Chia, R. Evans, M. J. Burek, M. Zhang, L. Wu, J. L. Pacheco, J. Abraham, E. Bielejec, M. D. Lukin, M. Atatüre, and M. Lončar, "Strain engineering of the silicon-vacancy center in diamond," Phys. Rev. B **97**, 205444 (2018).
[55] C. L. Panuski, I. Christen, M. Minkov, C. J. Brabec, S. Trajtenberg-Mills, A. D. Griffiths, J. J. D. McKendry, G. L. Leake, D. J. Coleman, C. Tran, J. St Louis, J. Mucci, C. Horvath, J. N. Westwood-Bachman, S. F. Preble, M. D. Dawson, M. J. Strain, M. L. Fanto, and D. R. Englund, "A full degree-of-freedom spatiotemporal light modulator," Nat. Photonics **16**, 834–842 (2022).
[56] A. J. Menssen, A. Hermans, I. Christen, T. Propson, C. Li, A. J. Leenheer, M. Zimmermann, M. Dong, H. Larocque, H. Raniwala *et al.*, "Scalable photonic integrated circuits for high-fidelity light control," Optica **10**, 1366–1372 (2023).
[57] W. Bogaerts, D. Pérez, J. Capmany, D. A. B. Miller, J. Poon, D. Englund, F. Morichetti, and A. Melloni, "Programmable photonic circuits," Nature **586**, 207–216 (2020).

[58]J. A. Zuber, M. Li, M. L. Grimau Puigibert, J. Happacher, P. Reiser, B. J. Shields, and P. Maletinsky, "Shallow silicon vacancy centers with lifetime-limited optical linewidths in diamond nanostructures," Nano Lett. **23**, 10901–10907 (2023).
[59]C. Wagner and N. Harned, "Lithography gets extreme," Nat. Photonics **4**, 24–26 (2010).
[60]M. Totzeck, W. Ulrich, A. Göhnermeier, and W. Kaiser, "Pushing deep ultraviolet lithography to its limits," Nat. Photonics **1**, 629–631 (2007).
[61]L. Li, L. D. Santis, I. B. W. Harris, K. C. Chen, Y. Gao, I. Christen, H. Choi, M. Trusheim, Y. Song, C. Errando-Herranz, J. Du, Y. Hu, G. Clark, M. I. Ibrahim, G. Gilbert, R. Han, and D. Englund, "Heterogeneous integration of spin–photon interfaces with a CMOS platform," Nature **630**, 70–76 (2024).